DOI: 10.13009/EUCASS2019-840



# Emergence and evolution of longitudinal structures on blunt cone nosetip in hypersonic flow

*Alexander V. Vaganov*, Anton Yu. Noev**, Vladimir N. Radchenko, Alexey V. Ledovskiy and Anna A. Maksimenko*
*Central Aerohydrodynamic Institute,*
*140180, Zhukovsky Str. 1, Zhukovsky, Russia*
**alexvaganov@yandex.ru*
***anton.noev@tsagi.ru*

## Abstract

Laminar-turbulent transition has been investigated in a shock tunnel at Mach number 5. Heat flux distributions on the cone surface have been obtained using temperature sensitive paint. For the larger nosetip bluntness it is found that thin longitudinal structures are formed in the nosetip region. For the smaller nosetips at the same freestream parameters the structures are not observed. The earliest observed structures are formed at the boundary layer edge Mach number lower than 0.4. At some distance downstream they turn into turbulent wedges. It is shown that the structures location is related to surface roughness rather than freestream disturbances.

## 1. Introduction

The present investigation is devoted to laminar-turbulent transition in hypersonic flow over slender blunt cone. Numerous experimental data on this topic are mainly limited to one of the following: relatively small nosetip bluntness, artificial surface roughness or measurements using discrete sensors. Among the rest of the data, most of which are summarized in [1], there are observations of transition on a “smooth” cone (or nosetip) which has no common theoretical [2–5] or physical [6] explanation up to date. Temperature sensitive paints technique, developed in the recent years, turned out to be much more informative tool than discrete sensors. The purpose of present work is to extend our previous investigations [7,8] to a higher nosetip bluntness.

## 2. Experimental set-up

The experiments have been carried out in the UT-1M shock tunnel operating by the Ludwieg scheme [9] at Mach number 5 and freestream unit Reynolds number $Re_\infty$ up to $9\times10^7$ per meter. The model is 6.5° half-angle cone with interchangeable sphere-conical nosetips. The length of the model without nosetip is about 330 mm. Nosetip radius values R = 5, 10, 15, 20 and 25 mm. External surfaces of the main model part (i.e. cone frustum) and nosetips are made from AG-4 material. Heat flux distributions over the model surface have been obtained using temperature sensitive paint [10]. Runs have been carried out varying nosetips as well as unit Reynolds number in account of pressure.

## 3. Results

The test matrix is shown in Table 1.

### 3.1 Cone frustum

Figure 1 shows distributions of measured relative intensity of paint luminescence in arbitrary units for the case of R = 5 mm nosetip. Range of the color scale is different for each figure to emphasize flow pattern in each case. The red and orange zones correspond to peak heating due to laminar-turbulent transition. The blue and purple zones are either laminar or transitional. Transition onset locations will be analyzed quantitatively later.

DOI: 10.13009/EUCASS2019-840



The distance between markers on cone frustum (63 mm) is shown in the capacity of a spatial scale; note, that the distances between markers on the nosetips in some cases are different from 63 mm. These markers are visible by naked eye points with known coordinates. They are specially applied to the model surface to be able to map two-dimensional camera images to each other. Subsequently their coordinates are used to map a resulted image to three-dimensional computer cone geometry.
At $Re_\infty = 1.71 \times 10^7$ m$^{-1}$ only the very beginning of transition is observed near model tail. At $Re_\infty = 3.93 \times 10^7$ m$^{-1}$ there is clearly transition end. With further increasing Reynolds number transition end moves upstream. There is notable angular asymmetry in the transition zone in contrast to turbulent zone.

Table 1: Test matrix

| Run number | Total pressure, ata | Total temperature, K | R, mm | Run number | Total pressure, ata | Total temperature, K | R, mm |
|---|---|---|---|---|---|---|---|
| 6976 | 60.20 | 466.4 | 25 | 7003 | 14.24 | 465.3 | 20 |
| 6977 | 49.02 | 461.6 | 25 | 7005 | 22.44 | 463.9 | 15 |
| 6978 | 38.31 | 466.5 | 25 | 7008 | 58.75 | 468.4 | 15 |
| 6979 | 26.73 | 468.5 | 25 | 7009 | 50.88 | 465.7 | 15 |
| 6980 | 13.28 | 464.8 | 25 | 7010 | 42.72 | 461.5 | 15 |
| 6993 | 42.46 | 469.7 | 5 | 7011 | 11.09 | 466.9 | 15 |
| 6994 | 27.30 | 463.5 | 5 | 7013 | 42.32 | 463.7 | 10 |
| 6995 | 11.85 | 462.1 | 5 | 7014 | 27.53 | 462.0 | 10 |
| 6996 | 63.01 | 463.1 | 5 | 7015 | 8.15 | 466.3 | 10 |
| 6998 | 50.08 | 468.4 | 5 | 7016 | 60.64 | 463.3 | 10 |
| 6999 | 59.33 | 467.5 | 20 | 7017 | 50.01 | 463.9 | 10 |
| 7000 | 52.06 | 463.0 | 20 | 7020 | 42.29 | 464.2 | 25 |
| 7001 | 37.97 | 465.0 | 20 | 7023 | 43.03 | 464.5 | 25 |
| 7002 | 27.70 | 468.9 | 20 | | | | |

Figure 2 shows the results for R = 10 mm. At $Re_\infty = 1.16 \times 10^7$ m$^{-1}$ whole visible flow region is laminar. As in the case of R = 5 mm nosetip, the rest four runs show upstream transition movement with increasing Reynolds number as well as asymmetry of transition zone in contrast to turbulent zone.
Figure 3 shows results for R = 15 mm. At $Re_\infty = 6.20 \times 10^7$ m$^{-1}$ thin longitudinal streak is visible between the spherical nosetip part and the transition zone near the middle model generatrix. At $Re_\infty = 7.27 \times 10^7$ m$^{-1}$ this streak is at the same location while at least two similar streaks emerged. These new streaks turn into turbulent wedges at some distance from the nosetip while the older one does not. At $Re_\infty = 8.32 \times 10^7$ m$^{-1}$ all three turn into turbulent wedges. Downstream the wedges spread, merge with each other and finally occupy the whole visible model surface. Thus, in this case transition on the whole visible model surface is due to the formation and instability of these three streaks.
The results for R = 20 and 25 mm, shown on Figures 4 and 5, are qualitatively similar to the case R = 15 mm. For the lowest Reynolds number whole visible model surface is laminar while for the highest Reynolds number transition to turbulence is determined by streaks. For the intermediate Reynolds number and R =20 mm it is hard to say whether streaks dominate over other transition mechanisms or not, like on Figure 5,b) and 5.c). However for R = 25 mm all observed turbulence is clearly due to streaks.
Note that a streak, emerged on the nosetip, could resist to transformation into turbulent wedge at a quite long distance – up to 15 nose radiuses (Figure 6,b)).

DOI: 10.13009/EUCASS2019-840



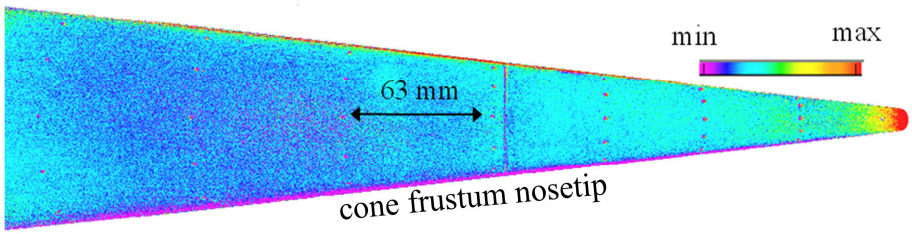


a) Run 6995, $Re_\infty = 1.71\times10^7$ 1/m;

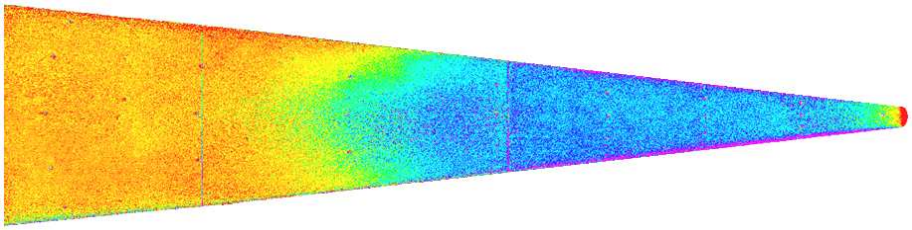

b) run 6994, $Re_\infty = 3.93\times10^7$ 1/m;

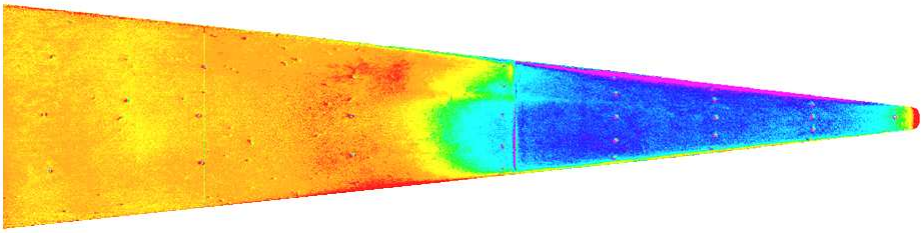

c) run 6993, $Re_\infty = 5.99\times10^7$ 1/m;

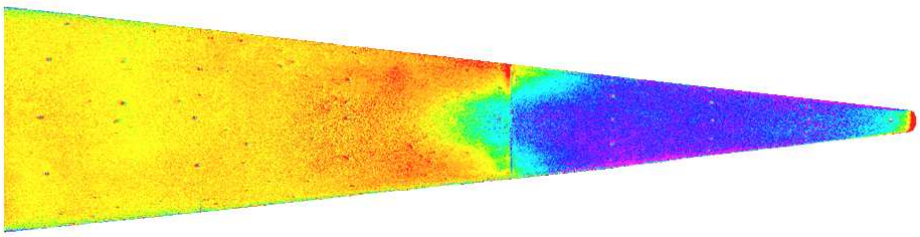

d) run 6998, $Re_\infty = 7.09\times10^7$ 1/m;

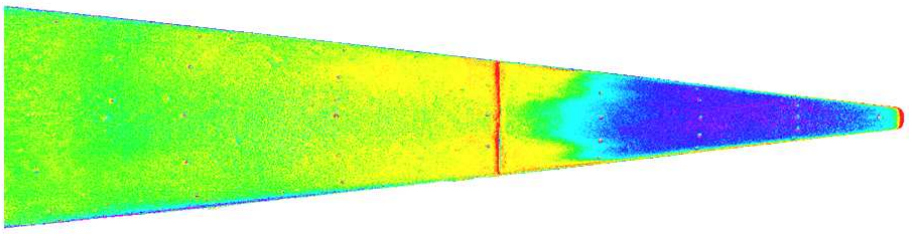

e) run 6996, $Re_\infty = 9.09\times10^7$ 1/m.

Figure 1: Distributions of relative luminescence intensity over cone surface. R = 5 mm. Flow direction is from the right to the left.

DOI: 10.13009/EUCASS2019-840



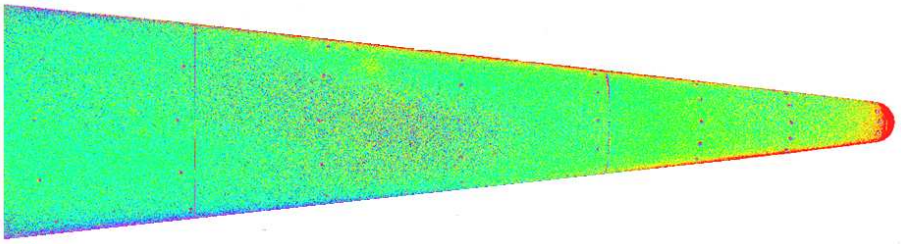

a) Run 7015, $Re_\infty = 1.16\times10^7$ 1/m;

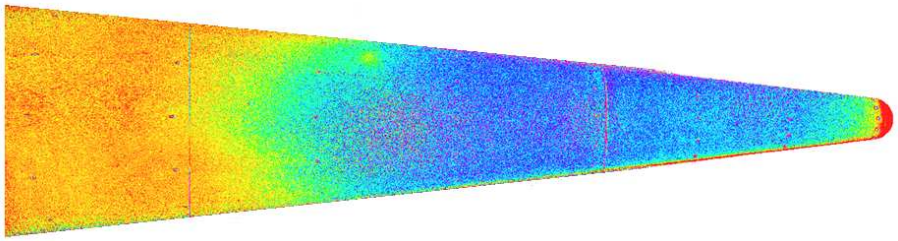

b) run 7014, $Re_\infty = 3.99\times10^7$ 1/m;

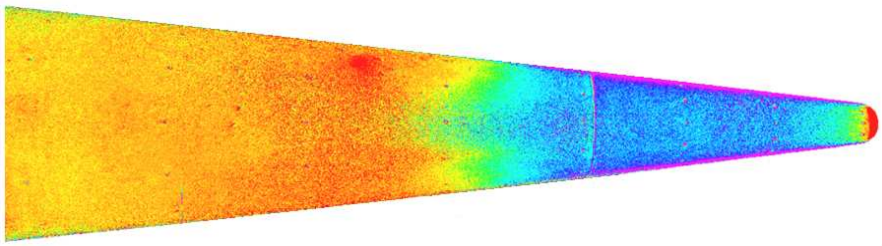

c) run 7013, $Re_\infty = 6.09\times10^7$ 1/m;

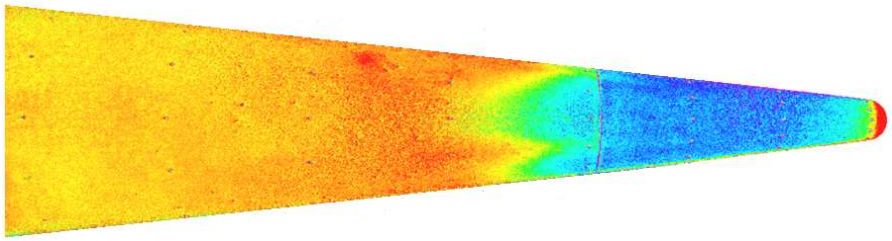

d) run 7017, $Re_\infty = 7.19\times10^7$ 1/m;

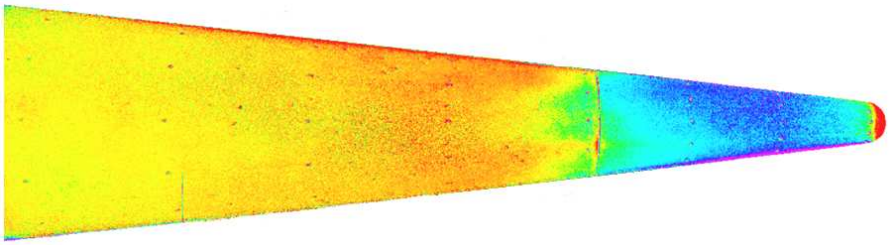

e) run 7016, $Re_\infty = 8.74\times10^7$ 1/m.

Figure 2: Distributions of relative luminescence intensity over cone surface. R = 10 mm.

DOI: 10.13009/EUCASS2019-840



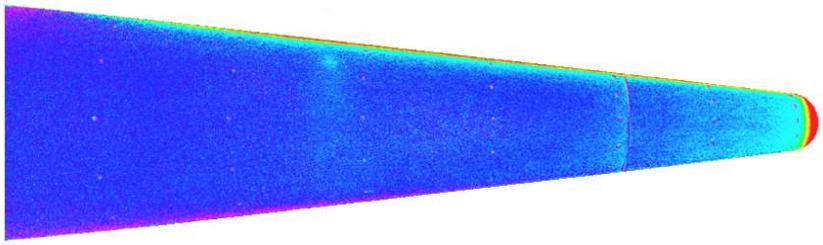

a) Run 7011, $Re_\infty = 1.58\times10^7$ 1/m;

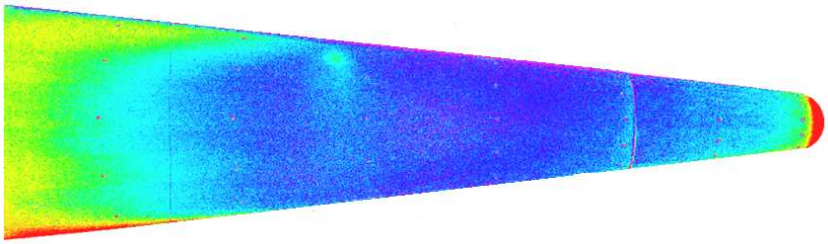

b) run 7005, $Re_\infty = 3.23\times10^7$ 1/m;

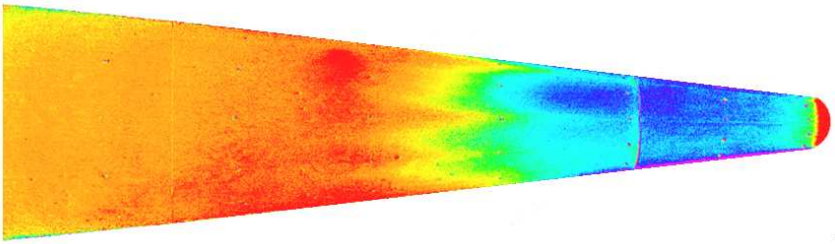

c) run 7010, $Re_\infty = 6.20\times10^7$ 1/m;

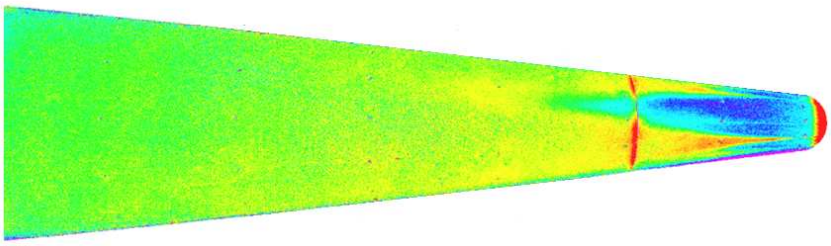

d) run 7009, $Re_\infty = 7.27\times10^7$ 1/m;

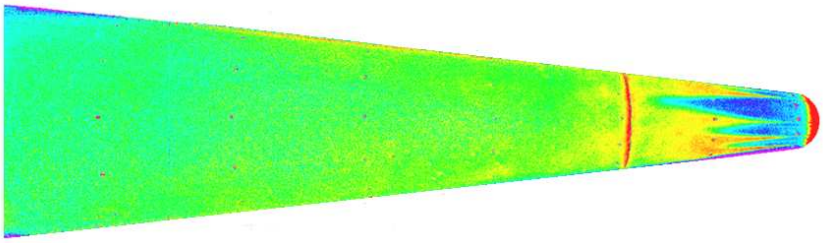

e) run 7008, $Re_\infty = 8.32\times10^7$ 1/m.

Figure 3: Distributions of relative luminescence intensity over cone surface. R = 15 mm

DOI: 10.13009/EUCASS2019-840



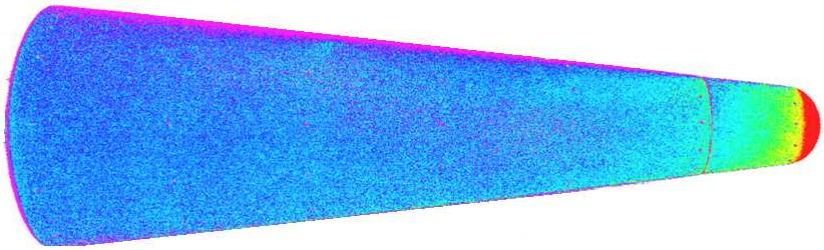

a) Run 7003, $Re_\infty = 2.04\times10^7$ 1/m;

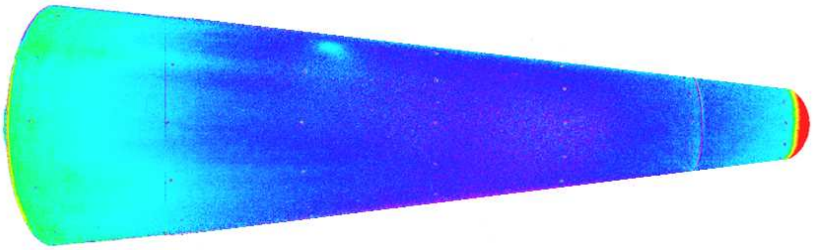

b) run 7002, $Re_\infty = 3.92\times10^7$ 1/m;

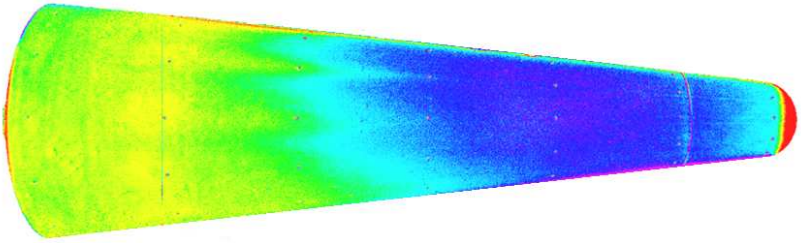

c) run 7001, $Re_\infty = 5.44\times10^7$ 1/m;

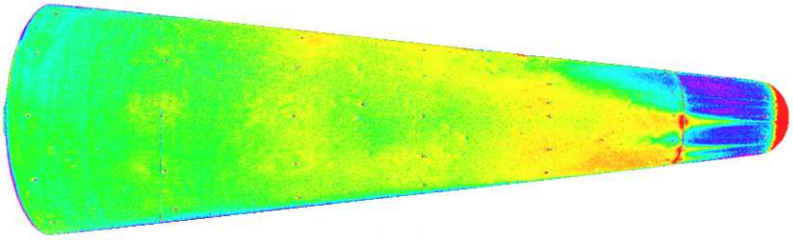

d) run 7000, $Re_\infty = 7.51\times10^7$ 1/m;

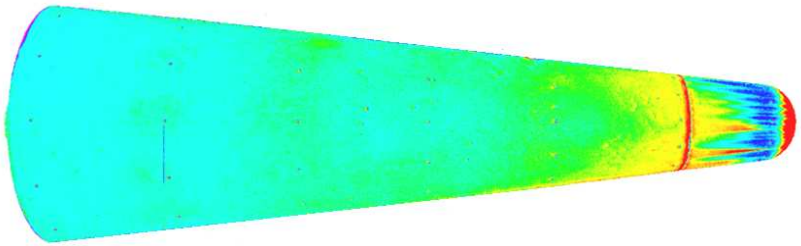

e) run 6999, $Re_\infty = 8.43\times10^7$ 1/m.

Figure 4: Distributions of relative luminescence intensity over cone surface. R = 20 mm

DOI: 10.13009/EUCASS2019-840



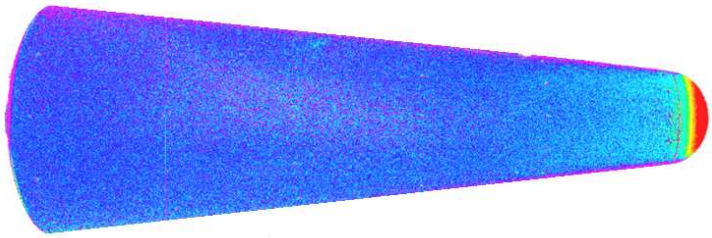

a) Run 6980, $Re_\infty = 1.90\times10^7$ 1/m;

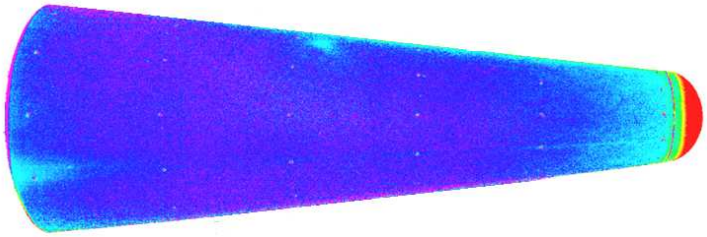

b) run 6979, $Re_\infty = 3.78\times10^7$ 1/m;

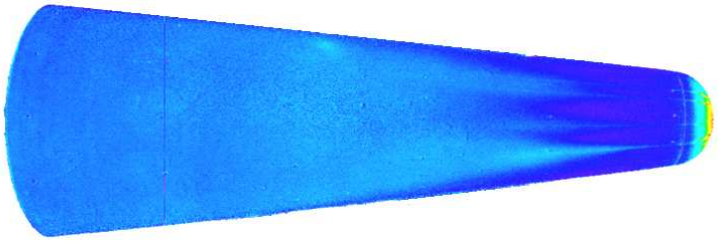

c) run 6978, $Re_\infty = 5.46\times10^7$ 1/m;

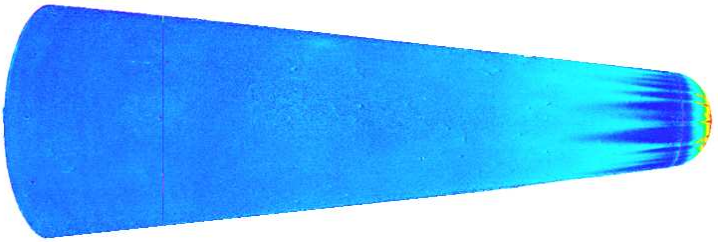

d) run 6977, $Re_\infty = 7.11\times10^7$ 1/m;

e) run 6976, $Re_\infty = 8.58\times10^7$ 1/m.

Figure 5: Distributions of relative luminescence intensity over cone surface. R = 25 mm.

DOI: 10.13009/EUCASS2019-840



### 3.2 Cone nosetip

In the end of the series two additional runs have been done. Before their conduction the cone has been shifted downstream so as cameras to view the nosetip rather than the frustum. On the nosetip R = 25 mm additional markers have been added for more accurate mapping of images. Before the second run, the cone has been rotated around its axis on 30°. The results are presented on Figure 6 and the new markers location is highlighted.

First, comparing Figure 6,a) and b) one can see that streaks rotated "together with the model". Consequently, their *location* is completely determined by the model properties (probably, distribution of roughness) rather than freestream disturbances. Unfortunately in the present investigation, roughness of the nosetip has not been measured due to limitations of available instrumentation. The model has been carefully polished before sensitive paint has been applied onto it. Tactile and visual examination revealed no observable local roughness, so one can estimate it less than 20 μm. Experiments with the same model and polished aluminium nosetips (their roughness will be measured) are in preparation at the moment.

Second, new markers are located at 20–25° from stagnation point depending on concrete marker (this uncertainty is due to they have been applied by hand without using precise instrumentation to avoid harming already applied paint; they have been excluded from two-to-three-dimensional images mapping, and have been used only for two-to-two-dimensional mapping, so that the uncertainty has no effect on final result.). Note that some streaks clearly originate somewhat upstream from the new markers. Calculation show that boundary layer edge Mach number at 20–25° from stagnation point is about 0.4. So, streaks can originate far upstream of sonic line, which is about 41° from stagnation point according to calculation.

Third, looking at, for example, Figure 6,b), one may naturally propose that the streak is produced by markers, since it goes right upon raw of them. It is possible if a marker is large enough and is working like isolated surface roughness. However on Figure 7 streaks 1 and 3 are located clearly between markers. Thus, markers are not necessary for occurrence of streaks.

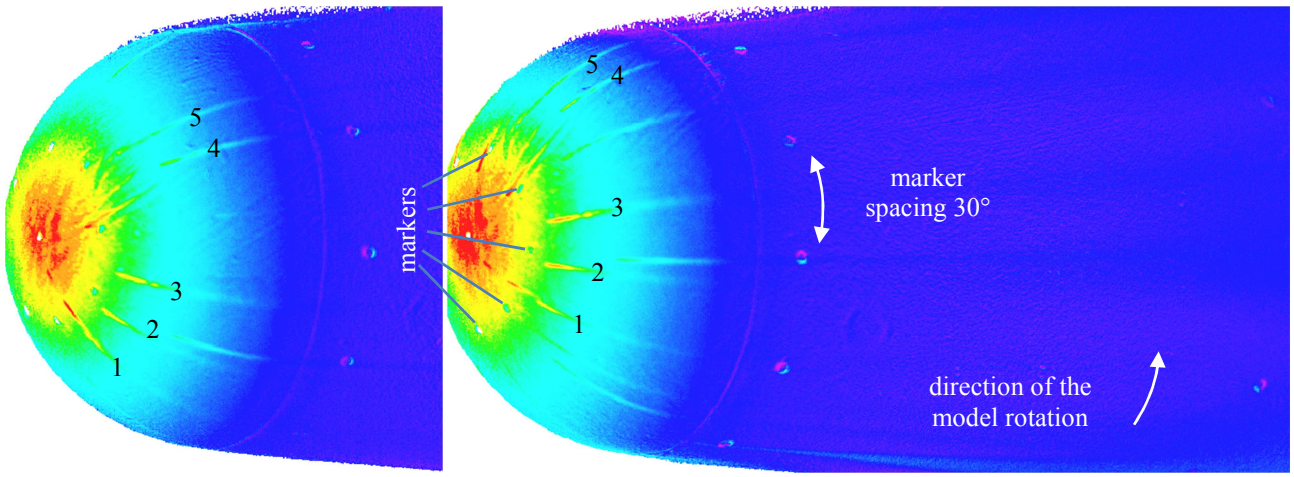


Figure 6: Streaks in nosetip region. R = 25 mm, flow from the left to the right. a) run 7020, $Re_{\infty R}$ =5.46×10$^5$; b) run 7023, $Re_{\infty R}$ = 5.55×10$^5$, the model is rotated around its axis on 30° counterclockwise to the flow relatively to the run 7020.

Similar streaks have been observed for example in [11–15]. In [11] they have been observed at relatively small roughness – 6.7 μm (Figure 10,a) from [11]). Figure 12 from [11] demonstrates non-monotone influence of roughness height on transition in the range of roughness size 4.8-6.7 μm. It is in agreement with the data [16] where increasing roughness led to decrease of heating on some part of sphere as well as with [17], where short review on influence of roughness on transition is given. In [12] they have been observed on "smooth" model. Though measurements of its roughness have not been presented, it should be less than that of the 230-mesh model, i.e. 17 μm. In [18] it is shown that depending on mutual location of two discrete roughness elements, disturbance, created by the upstream element, can stabilize as well as produce turbulent wedge. In [19] three identical models differing only by roughness size and shape has been tested in flight – the furthest transition has been observed on the most smooth model, though transition has occurred earlier on the model with mid-size roughness, than on the model with the largest roughness. In [20] transition has occurred upstream of the sonic point for R = 50.8 mm while flow

DOI: 10.13009/EUCASS2019-840



has been laminar for R=38.1 mm nosetip (both have had 0.05 μm roughness). According to [21], changing roughness height roughly from 0.5 to 0.05 μm significantly delayed transition.
In [22-24] significant influence of dust particles in freestream on model roughness and transition is discussed. Usually roughness is measured before experiments therefore actual roughness during experiments can significantly differ from reported value. The problem becomes even more complicated because usually reported mean height value does not adequately characterize roughness since from Figure 6 it seems that namely *local* peaks or tips are responsible for streaks. In view of above short review, it seems that though classical correlation parameters (like $Re_{kk}$, PANT and variations) seem to work good for relatively large roughness [25], combination of relatively small roughness with large bluntness and probably dust still deserves investigation.

### 3.3 Transition location

Transition beginning locations have been determined for each run on each of five model generatrixes: one locating along the middle of visible model part and others locating at ± 22.5 and ± 45° from it. Transition beginning location has been determined by the intersection of lines, corresponding to laminar and transitional flows (Figure 7).

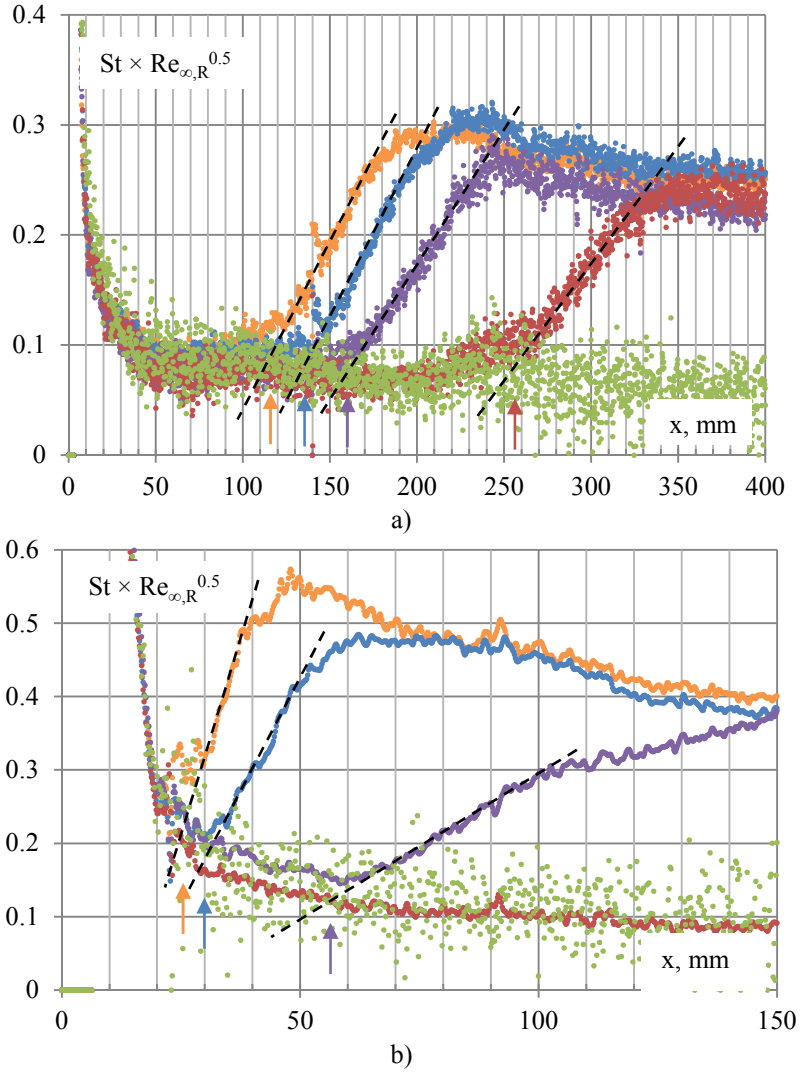


Figure 7: Heat flux distributions along the same generatrix at various Reynolds numbers; a) R = 10 mm, generatrix +45°; green points – $Re_{\infty,R} = 1.16\times10^5$, red – 3.99, violet – 6.09, blue – 7.19, orange – 8.74; b) R = 25 mm, generatrix +22.5°; green points – $Re_{\infty,R} = 4.76\times10^5$ , red – 9.46, violet –13.65, blue – 17.76, orange – 21.46. Arrows designate determined transition beginning locations.

To do this, one could extrapolate laminar part of the distribution for a concrete run downstream to the point where it would intersect with transitional line from the same run. However, due to very long transitional zones at large bluntness [26] and data scatter, this approach has showed oneself not very reliable, because it is hard to pick out the laminar region when looking at single run. Instead, in the present paper heat flux distributions at different Reynolds

DOI: 10.13009/EUCASS2019-840



number, other things being equal, are superimposed to each other in terms of $St \times Re_{\infty,R}^{0.5}$, St – Stanton number [10], $Re_{\infty,R} = \rho_\infty u_\infty R/\mu_\infty$, $\rho_\infty$, $u_\infty$, $\mu_\infty$ – freestream density, velocity and dynamic viscosity correspondingly.. This way, as is seen on Figure 7, laminar parts of distributions are in excellent agreement with each other. Transition is assigned at intersection of transitional curve with laminar curve from the run at minimal Reynolds number.
On Figure 7,a) the small local peak heating at $x \approx 100$ mm is observed for all curves, i.e. it does not depend on Reynolds number. This means that the peak is due to local irregularity of the model thermal properties rather than a flow feature or transition, as one may suppose when looking at single curve.
On Figure 7,b) both the red and green datasets corresponds to laminar flow, so transition is designated at intersection with the red line rather than the green line, due to less scatter.
The resulting Reynolds numbers and correlation [27] are shown on Figure 8.

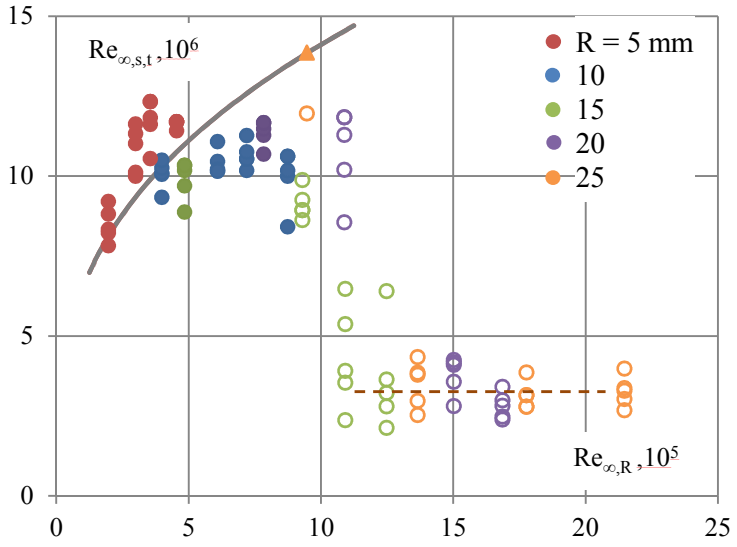


Figure 8: Transition beginning location Reynolds number in the present investigation ($M_\infty = 5$). Filled symbols – streaks are not observed, open symbols – streaks are observed. Triangle – laminar flow till the end of the model (Figure 6,b)). Solid line – correlation [27].

Transition in the run 6995 (Figure 1,a) is excluded from Figure 8 since there is only the very beginning of transition visible, therefore one cannot draw "transitional" line correctly. The correlation is used of the form $Re_{\infty,x,t} = 78825{,}5\ K^{0.64667}$, where $Re_{\infty,x,t} = \rho_\infty u_\infty x_t/\mu_\infty$, $x_t$ – axial distance from stagnation point to transition beginning location, $K = (Re_{\infty,R})^{0.5} \times M_\infty^2 \times \mathrm{Sin}(\theta)$, $M_\infty$ – freestream Mach, $\theta$ – cone half angle.
To better track early nosetip transition, data on Figure 8 are shown using s-coordinate rather than x, where s – distance from stagnation point along model surface (wetted length). $Re_{\infty,x,t}$ values given by the correlation have been converted to $Re_{\infty,s,t}$ using geometrical relations. Actually there are two solid lines on the Figure 8 – they correspond to R = 5 and 25 mm. One can see that they coincident with each other.
Data obtained are in good agreement with the correlation up to $Re_{\infty,R} \approx 5 \times 10^5$. Further up to $Re_{\infty,R} \approx 8 \times 10^5$ they deviate from the correlation though streaks are not observed (however they are not necessarily absent). It is similar to [8]. At $Re_{\infty,R}$ higher than $\approx 1.1 \times 10^6$ transition is always due to streaks giving $Re_{\infty,s,t} \approx 2\text{–}4 \times 10^6$ depending on generatrix choice. This value does not change at $Re_{\infty,R} \approx 1.1\text{–}2.2 \times 10^6$.
Data [28] have been obtained in the same shock tunnel the present investigation, however with different nozzle, flow temperature and model itself. At that model roughness before experiments have been probably similar since model preparation technique have been the same. Both datasets demonstrate occurrence of turbulent wedges produced by streaks . Original observations have been re-processed in the frame of the present investigation to exclude streak-dominated transition. The procedure is as follows. If there is possible for a given run to select a generatrix locating outside of turbulent wedges, then transition is determined by heat flux distribution along this generatrix, similar to [8]. Otherwise, the run is omitted. Transition location has been assigned at the beginning of rapid heat flux growth. The results are presented on Figure 9. Re-processed data agree with the correlation satisfactorily (though systematically demonstrate somewhat earlier transition), except three points, for which distributions of relative luminescence intensity is shown as on Figures 1–5. For the top right image the very beginning of transition is near the model end. If the model have been longer, transition would be assigned to the point of more rapid growth of heat flux, which would be somewhat downstream. This situation is similar to Figure 1,a). For the other two images hypothetically reversal occurs without streaks either streaks are not visible due do data noisiness.

DOI: 10.13009/EUCASS2019-840



In addition, data [29], taken from figure 1,a) from [30], are shown on Figure 9. They systematically demonstrate somewhat later transition, then than according to the correlation (until reversal occurs). Probably it is due to nosetip polishing before each run, rather than low level of noise, since FDL Mach 6 tunnel is not considered "quiet" [31].
Data, tabulated in [29] have been incorrectly used in [1] in comparison with the correlation – when calculating parameter K nosetip radius value have been supposed 3 mm while correct value is 1.5 mm. Correct comparison is shown on Figure 9.

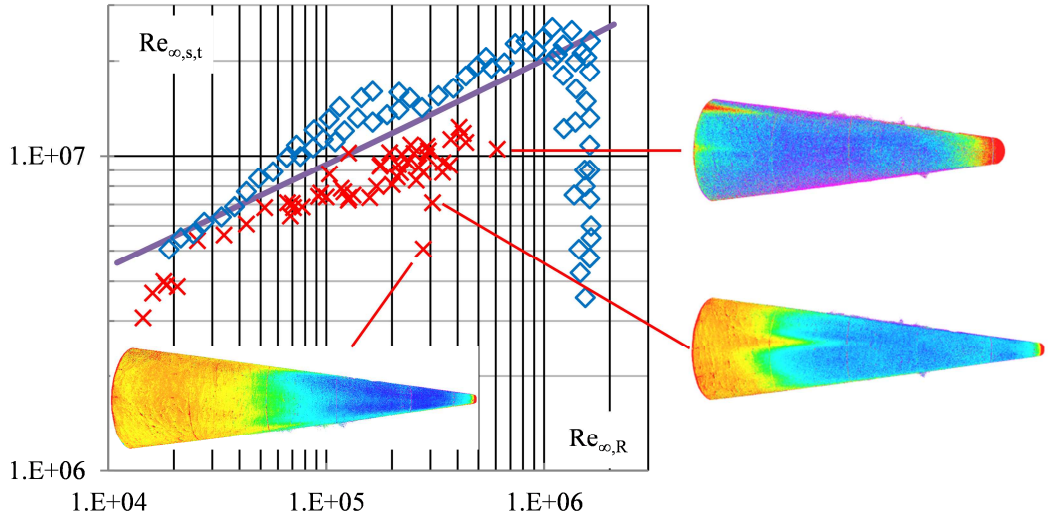


Figure 9: Re-processing (red crosses) of data [28] ($M_\infty = 6$); solid purple line – correlation [27]; blue diamonds – data [29].

## 4. Conclusions

At Reynolds number based on nosetip radius and freestream parameters $Re_{\infty,R}$ higher than roughly $9 \times 10^5$ thin longitudinal structures (streaks) are formed in the nosetip region, analogous to [11–15]. The earliest observed streaks are formed at the boundary layer edge Mach number lower than 0.4. At some distance downstream they turn into turbulent wedges. This distance decreases as Reynolds number increases. It is shown that streak location are related to surface roughness rather than freestream disturbances.
Data obtained are in good agreement with the correlation [27] up to $Re_{\infty,R} \approx 5 \times 10^5$. Further up to $Re_{\infty,R} \approx 8 \times 10^5$ they somewhat deviate from the correlation though streaks are not observed (however they are not necessarily absent). It is similar to [8]. At $Re_{\infty,R}$ higher than $\approx 1.1 \times 10^6$ transition is always due to streaks giving transition beginning Reynolds number $Re_{\infty,s,t} \approx 2–4 \times 10^6$. This value does not change at $Re_{\infty,R} \approx 1.1–2.2 \times 10^6$.
Data [28] have been re-processed to separate streak-dominated transition. Almost all originally reported data [28] corresponding to transition reversal regime are due to streaks. When such points are excluded, data [28] are in fair agreement with the correlation, though systematically demonstrate somewhat earlier transition.
Data [29] show somewhat later transition than correlation [27] (until reversal occurs), though agreement is fair. Hypothetically this is due to polishing of the model before each run rather than low level of noise, since FDL Mach 6 tunnel is not considered "quiet" [31].
Experiments with the same model and polished aluminium nosetips are in preparation.

## 5. Acknowledgements

The authors thank G.A. Trashkov, O.M. Manevich, A.V. Orekhov, D.A. Lozhkin and S.A. Anikin for designing, manufacturing and preparation of the model, N.B. Larin, S.I. Repin and N.P. Podymov for carrying out the experiments, T.V. Kubyshina for processing freestream parameters and NASA STI information desk personnel for scanning and making available online the report [20] at the instance of the authors.

## References

[1] Vaganov, A., A. Noev, V. Kashin and D. Grachikov. 2018. Scenarios of laminar-turbulent transition reversal on blunt cone in hypersonic flow. AIP Conf. Proc. 2027:030111-1–030111-5.

[2] Reshotko, E. 2001. Transient growth: A factor in bypass transition. *Phys. Fluids* 5:1067-1075.
[3] Marineau, E., C. Moraru, D. Lewis, J. Norris, J. Lafferty, R. Wagnild and J. Smith. 2014. Mach 10 boundary-layer transition experiments on sharp and blunted cones. AIAA Paper 3108.
[4] Fedorov, A. 1990. Instability of the entropy layer on a blunt plate in supersonic gas flow. *J. App. Mech. Tech. Phys.* 5:722-728.
[5] Jewell, J., R. Kimmel. 2016. Boundary layer stability analysis for Stetson's Mach 6 blunt cone experiments. AIAA Paper 598.
[6] Stetson, K. 1990. Comments on hypersonic boundary-layer transition. Wright Research and Development Center Technical Report 3057.
[7] Vaganov, A., A. Noev, V. Plyashechnik, V. Radchenko, A. Skuratov and A. Shustov. 2016. Laminar-turbulent transition on a blunted ogive-conical body at hypersonic speeds. AIP Conf. Proc. 1770:030049-1–030049-5.
[8] Vaganov, A, A. Noev, V. Radchenko, A. Skuratov and A. Shustov. 2017. Laminar-turbulent transition reversal on blunt ogive body of revolution at hypersonic speeds. In: *7th European Conf. for Aeronautics and Space Sciences*. DOI: 10.13009/EUCASS2017-120.
[9] Borovoy, V., A. Skuratov and E. Stolyarov. 2001. Pressure fluctuations in supersonic short- and long-duration wind tunnels. *TsAGI Sci. J.* 3–4:3–16. [in Russian] http://cyberleninka.ru/article/n/pulsatsii-davleniya-v-sverhzvukovyh-aerodinamicheskih-trubah-kratkovremennogo-i-dlitelnogo-deystviya
[10] Borovoy, V., V. Mosharov, A. Noev and V. Radchenko. 2012. Temperature sensitive paint application for investigation of boundary layer transition in short-duration wind tunnels. In: *Progress in Flight Physics*. 15-24.
[11] Wilder, M., D. Reda and D. Prabhu. 2015. Transition experiments on blunt bodies with distributed roughness in hypersonic free flight in carbon dioxide. AIAA paper 1738.
[12] Hollis, B. 2017. Experimental investigation of roughness effects on transition onset and turbulent heating augmentation on a hemisphere at Mach 6 and Mach 10. NASA Technical Memorandum 219613.
[13] Reda, D., M. Wilder, D. Prabhu. 2011. Transition experiments on slightly blunted cones with distributed roughness in hypersonic flight. AIAA Paper 3417.
[14] Leidy, A., E. Reshotko F. Siddiqui and R. Bowersox. 2017. Transition due to roughness on blunt capsule: comparison with transient growth correlation. *J. Spacecraft and Rockets* 1:167–180.
[15] Peterson, J. and E. Horton. 1959. An investigation of the effect of a highly favorable pressure gradient on boundary-layer transition as caused by various types of roughnesses on a 10-foot-diameter hemisphere at subsonic speeds. NASA Memorandum 2-8-59L.
[16] Irimpan, K., V. Menezes, K. Srinivasan and H. Hosseini. 2018. Nose-tip transition control by surface roughness on a hypersonic sphere. *J. Flow Control, Meas. & Vis.* 6:125–135.
[17] Choi, K. The rough with the smooth. 2006. *Nature* 6: 754.
[18] Suryanarayanan, S., D. Goldstein and G. Brown. 2019. Roughness induced transition: A vorticity point of view. *Phys. Fluids* 31:024101-1–024101-19.
[19] Rabb, L. and M. Krasnican. 1958. Effects of surface roughness and extreme cooling on boundary-layer transition for 15° cone-cylinder in free flight at Mach numbers to 7.6. NACA Research Memorandum E57K19.
[20] Krasnican, M. and L. Rabb. 1959. Effects of nose radius and extreme cooling on boundary-layer transition for three smooth 15°-cone-cylinders in free flight at Mach numbers to 8.50. NASA Research Memorandum 3-4-59E.
[21] Buglia, J. 1961. Heat transfer and boundary-layer transition on a highly polished hemisphere-cone in free flight at Mach numbers up to 3.14 and Reynolds numbers up to 24 x $10^6$. NASA Technical Note D-955.
[22] Dunlap, R. and A. Kuethe. 1962. Effects of cooling on boundary-layer transition on a hemisphere in simulated hypersonic flow field. *J. Aero. Sci.* 12:1454–1461.
[23] Holden, M. 1985. Studies of potential fluid-mechanical mechanisms for enhanced stagnation-region heating. AIAA Paper 1002.
[24] AIAA. 1986. Thermophysical aspects of re-entry flows. Progress in astronautics and aeronautics 103.
[25] Polivanov, P., Yu. Gromyko and A. Maslov. 2018. Study of interference of two roughness wakes for compressible flow. AIP Conf. Proc. 2027:040047-1–040047-5.
[26] Zanchetta, M. 1996. Kinetic heating and transition studies at hypersonic speeds. PhD thesis. University of London.
[27] Brazhko, V., A. Vaganov, N. Kovaleva, N. Kolina and I. Lipatov. 2009. Experimental and numerical investigations of boundary layer transition on blunted cones at supersonic flow. *TsAGI Sci. J.* 3:1-11.
[28] Aleksandrova, E., A. Novikov, S. Utyuzhnikov and A. Fedorov. 2014. Experimental investigation of laminar-turbulent transition on blunted cone. *J. App. Mech. Tech. Phys.* 3:5-16.
[29] Stetson, K. 1983. Nosetip bluntness effects on cone frustum boundary layer transition in hypersonic flow. AIAA Paper 1763.

DOI: 10.13009/EUCASS2019-840



[30] Paredes, P., M. Choudhari, F. Li, J. Jewell, R. Kimmel, E. Marineau and G. Grossir. 2018. Nosetip bluntness effects on transition at hypersonic speeds: experimental and numerical analysis under NATO STO AVT-240. AIAA paper 57.
[31] Stetson, K. 1980. Hypersonic boundary layer transition experiments. AFWAL Technical Report 3062.